

## Metamaterial Analogues of Strongly Coupled Molecular Ensembles

Milo Baraclough, Ian R. Hooper, and William L. Barnes\*

Cite This: *ACS Photonics* 2021, 8, 2997–3003

Read Online

ACCESS |



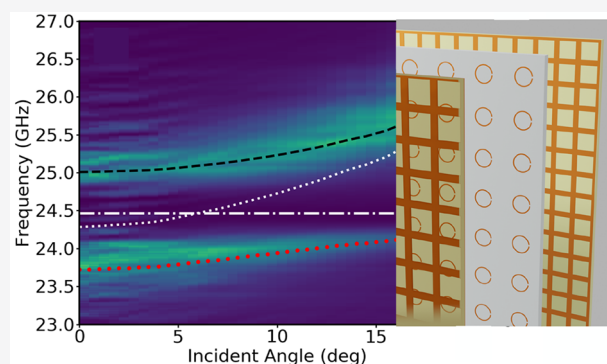
Metrics &amp; More



Article Recommendations

**ABSTRACT:** The formation of polariton modes due to the strong coupling of light and matter has led to exciting developments in physics, chemistry, and materials science. The potential to modify the properties of molecular materials by strongly coupling molecules to a confined light field is so far-reaching and so attractive that a new field known as “polaritonic chemistry” is now emerging. However, the molecular scale of the materials involved makes probing strong coupling at the individual resonator level extremely challenging. Here, we offer a complementary approach based upon metamaterials, an approach that enables us to use cm-scale structures, thereby opening a new way to explore strong coupling phenomena. As proof-of-principle, we show that metamolecules placed inside a radio frequency cavity may exhibit strong coupling and show that near-field radio frequency techniques allow us, for the first time, to probe the response of individual metamolecules under strong coupling conditions.

**KEYWORDS:** strong coupling, metamaterials, Rabi splitting, polariton, microcavity, polaritonic chemistry



An embryonic new field is emerging based upon the concept of hybrid states that are part light, part matter; these states are known as polaritons. This new field, known as “polaritonic chemistry”, arises from the opportunities such hybridization offers to explore and exploit new phenomena and new materials.<sup>1–6</sup> Most attention has been focused on light that is in the visible or infrared part of the spectrum. When this light is hybridized with excitonic (molecular) resonances, exciton-polaritons are formed;<sup>7</sup> when molecular vibrational or lattice phonon resonances are involved, then vibro-<sup>8,9</sup> and phonon-polaritons<sup>10,11</sup> are formed. The attraction of this mixing of light and matter has previously led to developments such as polariton lasers<sup>12</sup> and Bose–Einstein condensation,<sup>13–15</sup> while the rapid rise of interest in polaritonic chemistry derives from the fact that strong coupling has been reported to lead to modified chemical reaction rates,<sup>16–18</sup> modified intermolecular energy transfer,<sup>19–21</sup> modified exciton transport,<sup>22,23</sup> altered phase transitions,<sup>24</sup> and a potential reordering of singlet–triplet energies.<sup>25–27</sup>

Mixing light and matter in this way typically involves coupling the electric dipole moments associated with molecules—for example, an excitonic transition—to a confined light field. An archetypal example is that of placing a large number of dye molecules inside a planar microcavity.<sup>7</sup> If the molecular dipole moments exchange energy with the confined light field at a rate that is greater than any other (dissipative) rate, then hybridization ensues, and one is in what is known as the strong coupling regime.<sup>27–29</sup> While a great deal has been

done in this area, much of it is sparked by the pioneering work of the Ebbesen group over the past decade,<sup>1</sup> a great deal still remains to be understood.<sup>30,31</sup>

The visible and infrared wavelengths of the light involved in these fascinating phenomena mean that the spatial scale of the structures used in these experiments is necessarily small. Consequently, while one would ideally probe these systems at the molecular level to investigate the precise nature of the light-matter hybridization, this is not really feasible.<sup>32</sup> Among the questions one would like to explore are the effect on individual (molecular) resonators of strong coupling, the detailed effects of disorder, the role of dark states, and the degree of spatial coherence of the polariton states.

With these questions in mind, we sought to open up a new avenue to address some of these matters by making use of a radio frequency (RF) metamaterial analogue. There are various reports of coherent coupling phenomena at THz and RF frequencies; however, these either do not deal with ensemble strong coupling, i.e., situations where there are a large number of metamolecules, but instead deal with single meta-atoms;<sup>33</sup> are based on molecular rather than metamolecular responses;<sup>34</sup>

Received: June 22, 2021

Published: September 20, 2021

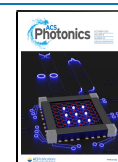


exhibit coherent coupling but do not demonstrate strong coupling;<sup>35</sup> or exhibit strong coupling but do not do so in a system with which it is easy to mimic the optical experiments discussed above.<sup>36</sup> Our approach here is to employ electromagnetic metamaterials<sup>37,38</sup> to mimic the optical experiments as closely as possible. Previously we have shown how metamolecules can be successfully used to create analogues for molecular aggregates,<sup>39</sup> while others have used a similar approach to successfully explore RF analogues of intermolecular energy transfer.<sup>40</sup> Our objective here is to establish through proof-of-principle a metamaterial analogue that may allow a complementary set of studies to be made on strong coupling phenomena.

In the work reported here, we sought to use our metamaterial analogue to replicate the anticrossing of a molecular resonance and a cavity mode. We also set out to directly probe the character of the polaritons by making use of another advantage of the metamaterial analogue approach, that of being able to map the electromagnetic near-fields inside the cavity. Probing the strong coupling phenomenon by making measurements inside the cavity has not been reported before and is a unique advantage of the RF metamaterial approach.

## RESULTS

To investigate the use of metamaterials as analogues for molecular strong coupling, two key components are required: a planar Fabry-Pérot cavity suitable for GHz frequencies and a set of metamolecules to place inside the cavity. For the mirrors, we used copper wire meshes, and for the metamolecules, we used split-ring resonators (SRRs),<sup>41</sup> see Figure 1. Let us look briefly at the mirrors and resonators in turn.

The cavities used in strong coupling experiments in the visible and infrared parts of the spectrum frequently make use of mirrors based on simple metal films.<sup>9,42–45</sup> These metal films are typically 30 nm or so thick, a thickness comparable with the skin depth. At this thickness, they are highly reflecting

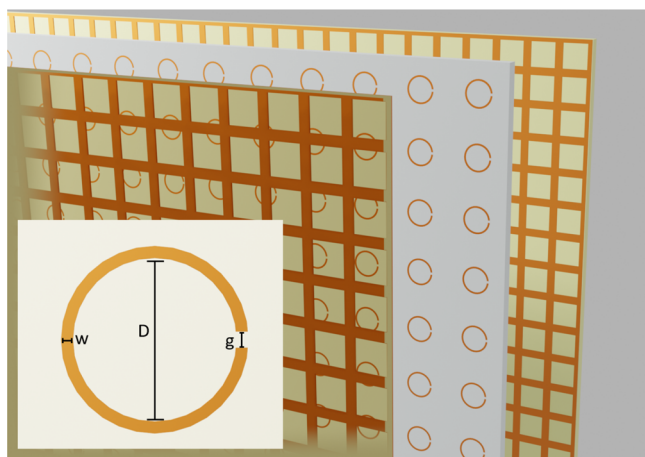


**Figure 1.** Metamaterial cavity and metamolecules. The schematic shows a cavity made from two mesh/grid mirrors, between which is a sheet of metamolecules. The mirrors are formed of a copper grid on a dielectric substrate with a grid period of 1.5 mm and an aperture size of 1.25 mm. The metamolecules are copper split-ring resonators, also on a dielectric substrate. The inset shows the dimensions of a single split-ring resonator:  $w = 0.15$  mm,  $D = 1.1$  mm,  $g = 0.1$  mm. The mirrors were 300 mm  $\times$  300 mm in area, and the mirror separation was 29 mm. All metallic regions were 35  $\mu$ m in thickness.

but still provide some degree of field penetration, allowing the incident light to be coupled in to the modes of the cavity. Such an approach is not suitable at the GHz frequencies associated with the radio frequency RF range owing to the very large impedance mismatch between metals and air at these frequencies. For an operating frequency of  $\sim 25$  GHz—the center of our chosen frequency band—a continuous metal film would need to be of order only 1 nm thick to provide the same degree of transmission as is commonly achieved at optical frequencies. Instead, the cavities used in this work were based on metallic mesh mirrors; see the [Methods](#) section.

We chose to work with a cavity having a spacing between the mirrors of 29 mm. This choice of cavity thickness means that it is the fifth-order mode that occurs at  $\sim 25$  GHz. While it might seem better to work with a cavity thickness that results in 25 GHz being the frequency of the lowest-order mode, such a cavity would be only  $\sim 5$  mm across, and this would not provide the space needed to include both our metamolecules and our near-field probes.

For the metamolecules, we used the well-established splitting resonators,<sup>46</sup> as shown in the inset of Figure 1; further details are given in the [Methods](#) section.

Two characterization techniques were used in this work to probe the far- and near-field responses of our system. To characterize the far-field angle-dependent response, the cavity was placed on a rotating stage between two horn antennas, with the transmission between the antennas being measured using a vector network analyzer (VNA) as the sample was rotated. To look at the effect of the metamolecules on the transmission through the cavity, the electric field of the incident radiation was aligned parallel to the direction joining the ends of the splits.

The near-field response was characterized by exciting the cavity at a fixed angle of 15.5 degrees using a horn antenna and measuring the transmission between the horn antenna and a wire antenna mounted within the cavity. The wire antenna was then scanned in a raster pattern in the plane of the resonator sheet in both  $x$ - and  $y$ -directions to map out the response across the sheet.

Angle-dependent far-field transmission data were acquired for three different configurations: the empty cavity; the sheet of SRR metamolecules on their own, i.e., outside the cavity; and the cavity filled with the sheet of SRR metamolecules. Transmission data were acquired for a range of incident angles between  $0^\circ$  and  $20^\circ$ . Example data are shown in Figure 2a for the “empty” cavity (see [Methods](#)) and the filled cavity; these data are for an angle of incidence of  $6.5^\circ$ .

The data for the empty cavity show two transmission peaks at  $\sim 20.5$  GHz and  $\sim 24.5$  GHz; these are the fourth- and fifth-order cavity modes, respectively. For the filled cavity, the fourth-order mode still shows as a single peak, similar to that for the empty cavity. This is as expected; the SRRs are not resonant at this frequency, and furthermore, the fourth-order mode has an electric field node at the cavity center, where the metamolecules are located. However, the fifth-order mode shows a very clear splitting. This splitting can be understood by looking at the data in panel b) of Figure 2, where the transmittance is shown as a function of the incident angle for the filled cavity. The oscillations in the data at low incident angles (visible in Figure 2b up to  $\sim 6^\circ$ ) are due to interference between the incoming signal and the back reflection from the cavity; at higher incidence angles reflection from the cavity is not directed back to the source.

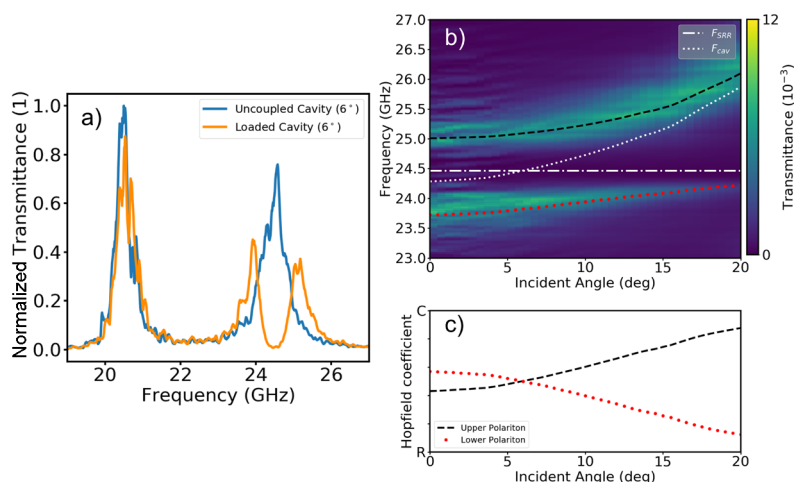


**Figure 2.** Strong coupling in the metamaterial cavity. (a) Transmission spectra at 6.5 degrees for both the “empty” and “filled” cavities. (b) Transmission through a 29 mm cavity filled with SRRs as the incident angle is swept between 0 and 20 degrees. Plotted in white are the uncoupled mode positions of the resonators ( $F_{\text{SRR}}$ ) and the cavity ( $F_{\text{cav}}$ ). Plotted in black and red are the calculated upper and lower polariton modes, respectively. (c) Plot of the Hopfield coefficients for the upper and lower polariton modes as the incident angle is swept between 0 and 20 degrees. The coefficients are plotted between R, which represents a fully SRR-like mode, and C, which represents a fully cavity-like mode.

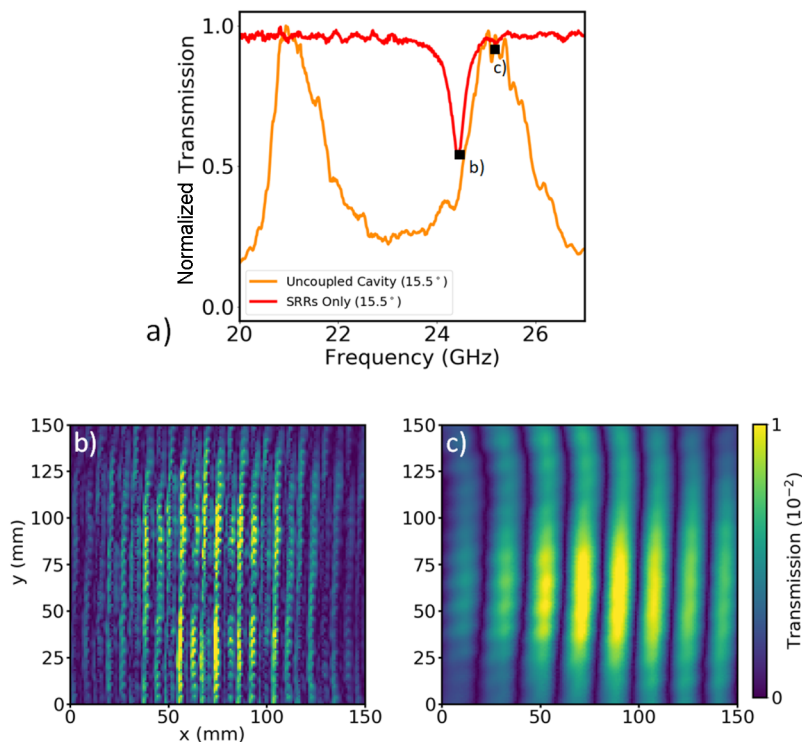


**Figure 3.** Probing the cavity-only and metamolecule-only systems. The panels are as follows: (a) far-field transmission spectra at a 15.5° angle of incidence for cavity-only and SRR-only systems, the frequencies at which the cavity-only (25.42 GHz, panel c) and SRR-only (24.47 GHz, panel b) near-field plots were obtained are indicated; (b) near-field map of the sheet of resonators; and (c) near-field map inside the empty cavity. For the near-field maps, the plotted quantity (transmission) is proportional to the magnitude of the instantaneous electric field strength; see [Methods](#) for details.

In panel b) of [Figure 2](#), the measured frequency of the SRR metamolecule resonance is indicated by the white dash-dotted line, while the measured (angle-dependent) frequency of the empty cavity is indicated by the white dotted line. The frequency of the empty cavity mode matches that of the metamolecule resonance when the angle of incidence is  $\sim 6.5^\circ$ , and it can be seen from the transmittance data for the filled cavity (color map) that there is an anticrossing. This

anticrossing is the key feature of strong coupling; it is one of the major results from our investigation.

To check that we are in the strong coupling regime, we need to determine the extent of the anticrossing, i.e., the frequency separation,  $\Omega$ , and compare it with the width of the bare cavity mode,  $\Delta\omega_{\text{cav}}$  and the width of the bare resonator modes,  $\Delta\omega_{\text{SRR}}$ . More specifically, we need to check whether  $\Omega > \Delta\omega_{\text{cav}} + \Delta\omega_{\text{SRR}}$ <sup>47,48</sup> since this is perhaps the most stringent criterion



for strong coupling. We determined the widths as follows:  $\Delta\omega_{\text{cav}} = 0.57 \pm 0.02$  GHz and  $\Delta\omega_{\text{SRR}} = 0.38 \pm 0.04$  GHz, so that  $\Delta\omega_{\text{cav}} + \Delta\omega_{\text{SRR}} = 0.95 \pm 0.05$  GHz. The splitting is determined by the frequency separation of the new hybrid modes at what, in the absence of coupling, would be the crossing point, i.e., at an angle of incidence of  $6.5^\circ$ . From the data in Figure 2(b), we find the splitting to be  $\Omega = 1.25 \pm 0.13$  GHz, significantly greater than the sum of the line widths; we are thus in the strong coupling regime.

Strong coupling involves the formation of hybrid polariton modes, and one indication of this comes from looking at the dispersion of the modes and the observation of an anticrossing, as we have seen in Figure 2. In addition, it is both interesting and informative to look at the hybrid nature of the strongly coupled modes and specifically to explore the relative proportion of their light/matter content. In the optical regime, this has not so far been directly possible. However, as we show here, our metamaterial analogue approach opens up such an opportunity. We will discuss directly probing this aspect by experiment later, but before doing so we will focus on indirectly calculating the light/matter content of these hybrid modes using a simple toy model for the hybridization.

A convenient technique for predicting the degree of hybridization expected in a system such as that explored here is to make use of a simple coupled oscillator model.<sup>29,49</sup> The flat-band nature of the resonator-only response indicates that the interaction between the SRR resonators is very small (the field of the resonators is highly localized), and the coupled oscillator model for the system can thus be represented as (1)

$$\begin{bmatrix} F_{\text{cav}} & \Omega \\ \Omega & F_{\text{SRR}} \end{bmatrix} \cdot \begin{bmatrix} x_1 \\ x_2 \end{bmatrix} = \lambda \begin{bmatrix} x_1 \\ x_2 \end{bmatrix} \quad (1)$$

where  $F_{\text{cav}}$  is the resonance frequency of the empty cavity,  $F_{\text{SRR}}$  is the resonance frequency of the bare SRRs, and  $\Omega$  is the coupling strength between the two.  $x_1$  and  $x_2$  make up an eigenvector of the system, while  $\lambda$  is a corresponding eigenvalue. The eigenvalues of this matrix are the frequency positions of the upper and lower polaritons of the coupled system, while the components of the eigenvectors ( $x_1$  and  $x_2$ ) are the Hopfield coefficients; in our case, these give the degree of “cavity-like” and “metamolecule-like” character of the polaritons. By choosing a value of  $\Omega$  that fits the polariton modes to those measured in experiment, we can derive the degree of mode hybridization between the resonators and the cavity from the eigenvectors. Figure 2c shows the results of the Hopfield analysis on our system. The upper polariton changes from being more SRR-like at normal incidence to almost entirely cavity-like at  $20^\circ$  and vice versa for the lower polariton.

Let us turn now to the experimental data relevant to directly probing the character of the measured polariton modes. Figure 3 is for the empty cavity and metamolecules only, while Figure 4 is for the filled cavity. All near-field measurements were undertaken at an angle of incidence of  $15.5^\circ$ , where the coupled oscillator model indicates that the upper polariton is 74.6% cavity-like and the lower polariton is 25.4% cavity-like.

Let us look first at the two component systems, i.e., the cavity and the resonators, Figure 3. Panel a) shows two spectra, taken at an angle of incidence of  $15.5^\circ$ , one for the empty cavity (orange) and one for the array of metamolecules on their own (red). Panel b) shows a near-field scan of the bare SRRs at the SRR resonance frequency, while panel c) shows a near-field scan for the empty cavity at a frequency

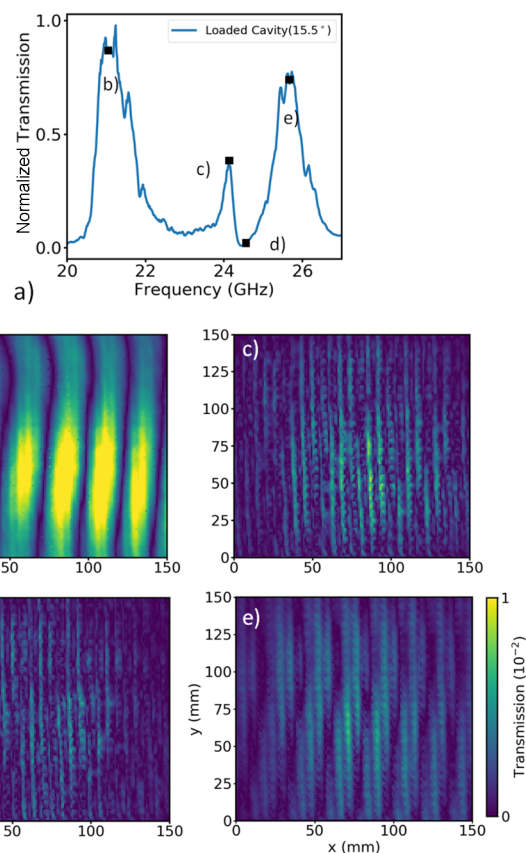


**Figure 4.** Probing the polariton character inside the cavity The spectrum for the filled cavity, again at a  $15.5^\circ$  angle of incidence, is shown in panel a), the frequencies at which the near-field maps in the remaining panels were acquired are indicated in this plot: (b) near-field map for the fourth-order cavity mode (21.0 GHz); (c) near-field map for the lower polariton (24.12 GHz); (d) near-field map at the frequency of the bare SRR resonance (24.47 GHz); and (e) near-field map for the upper polariton (25.5 GHz). As predicted by the Hopfield analysis at  $15.5^\circ$  (see Figure 2c), the two polaritons share both cavity and SRR-like features though to very different degrees, with the lower polariton being SRR-like and sharing many features with the measurement of the bare SRRs, while the upper polariton has SRR-like features but predominately resembles the empty cavity in the near-field profile. For the near-field maps, the plotted quantity (transmission) is proportional to the magnitude of the instantaneous electric field strength; see Methods for details.

corresponding to the fifth-order mode. The near-field scans are plotted as color scales, the color indicating the strength of the detected instantaneous electric field as a function of position. In panel b), excitation around the bare SRRs is highly localized to the neighborhood of the resonators. The streaks in these data in the  $y$ -direction are due to the smearing effect resulting from the finite size of the near-field probe antenna which is elongated in the  $y$ -direction. In the  $x$ -direction, it is clear that there is little to no interaction between neighboring resonators. In the empty cavity data, panel c), we see clear bands (oscillations) arising from the in-plane propagating nature of the cavity mode. The bands observed here, with a spacing of 44.2 mm, are consistent with the fields inside the cavity being excited at an angle of incidence of  $15.5^\circ$ . Note that the bands are not standing waves, rather they correspond to traveling waves (cavity modes); they appear as standing waves

here because we have plotted the instantaneous electric field, see [Methods](#).

Let us now look at the combined system, for which data are shown in [Figure 4](#). At the top, we again present a line spectrum, this time for the SRR-filled cavity. Four frequencies of interest are indicated as b), c), d), and e)—referring to the near-field maps shown in panels b), c), d), and e); let us look at each of these in turn. The fourth-order mode (b) of the filled cavity is very similar to the data for the empty cavity, panel c) of [Figure 3](#)), although with the change in frequency in going from a fifth-order mode to a fourth-order mode comes a change in the period of the oscillations from 44.2 to 53.4 mm. Despite being filled with the SRR array, there are no signs of hybridization, only small perturbations in the field when the detecting antenna is in close proximity to the metal resonators. Panel d) shows a near-field map for a frequency that matches the resonance of the bare SRRs. Despite the near-zero transmission at this frequency (see panel a)) we can see that the SRRs are nonetheless excited and that there is very little indication of any hybridization with a cavity mode. Panels c) and e) show near-field scans at the frequency of the lower and upper polariton modes for this angle of incidence. From the Hopfield analysis described above, we can expect a high degree of SRR-like features in (c), while we should expect cavity-like features in (e). This is indeed the case with the lower polariton mode being primarily similar in form to the bare SRRs (fields are localized around the resonators) but with a slight modulation in the *x*-direction from the cavity mode, while the upper polariton mode appears to look like a cavity mode perturbed by the presence of the SRRs.

## DISCUSSION

We have shown that metamaterials can be used to construct an analogue of a very topical and important class of structures based on the concept of strong coupling between molecules and confined light fields. We have developed a system to investigate the coupling between a Fabry-Pérot mode supported by a cavity formed from metallic mesh mirrors and the localized resonances supported by a sheet of metamolecules based on split-ring resonators. With this system, we have shown that an anticrossing between the cavity mode and the metamolecule resonance can be achieved and that the extent of the mode splitting between the hybrid polariton modes satisfies the most stringent of strong coupling criteria. We have then exploited a key feature of working at GHz frequencies—that of being able to directly probe the RF near-field—to look at the mixed light/matter character of the polariton modes, finding good agreement with what is expected on the basis of a well-established coupled oscillator model. We should note that our analogue system is only that, an analogue; there will be effects that are not open to study with such an approach.

We hope that this demonstration of a metamaterial analogue for strong coupling will act as a springboard for further work. For example, it should be relatively straightforward to investigate the effect of changing the areal density of resonators and to examine the effect of the size (area) of the cavity.<sup>50</sup> A more in-depth study of the near-fields inside the cavity, comparing their strength with that of the transmitted field, may help build up a better picture of the relationship between the fields inside strongly coupled cavities and the far-fields.<sup>51</sup> The addition of disorder to the metamaterial layout, either spatially or through slight variations in shape/size of resonators,<sup>52</sup> is

another obvious route for a future investigation. Combining near-field measurements with disorder might perhaps offer a way to learn something about the localization lengths associated with dark modes.<sup>53–55</sup> The use of more complex metamolecules with multiple dipole moments may provide an interesting way to probe more complex systems, while the incorporation of electronic components might allow the effect of noise to be mimicked. We also note that this metamaterials approach could be applied to other types of confined light field, including open cavities exploiting surface waves<sup>56</sup> and cavity-free geometries.<sup>57</sup>

## METHODS

All the samples used in this paper were fabricated using standard commercial PCB wet-etching techniques by the company Multi Circuit Boards and had a copper thickness of 35  $\mu\text{m}$ .

**Cavity.** Each of the mirrors was formed from a dielectric panel 300 mm  $\times$  300 mm in area (substrate material FR4, thickness 1.55 mm), upon which there was a square copper mesh (mesh period 1.5 mm, the mesh wires being 0.25 mm wide and 35  $\mu\text{m}$  thick, see [Figure 2](#)). The transmittance of the meshes across our chosen frequency band was  $\sim 25\%$ .

**Metamolecules.** The SRRs had an outer radius of 0.7 mm, a ring width of 0.15 mm, and a gap size of 0.1 mm. These parameters give the SRRs a first-order resonance frequency of 24.47 GHz when printed on a (dielectric) Rogers 4350B substrate. In this study, we chose an orientation for the incident electric field such that only the electric dipole moment was excited. This choice still results in a magnetic moment being induced by currents circulating in the ring;<sup>58</sup> but because this moment is perpendicular to the magnetic fields in the cavity, it does not contribute to the subsequent interaction. The SRRs were printed so that the spacing between the center of each resonator was 6 mm, enabling 2500 resonators to be produced on a single sheet. The period of the arrays was chosen so as to ensure that any diffractive effects occur at frequencies higher than those studied here. At this spacing, the interaction between the resonators is small, the primary affect being a modest increase in resonance line width rather than a shift in resonance frequency; this is comparable to observations made elsewhere.<sup>59</sup>

**All RF Measurements.** All measurements were taken using an Anritsu Vectorstar MS4644A Vector Network Analyzer (VNA) connected via 50  $\Omega$  coaxial cables to the interrogative antennas. In the case of the far-field measurements, two bespoke, lens-type horn antennas (Flann Microwave, Ltd.) served this purpose. Each had a 3 dB beam-width of 5.7 deg in the E-plane and 6.6 deg in the H-plane. Far-field data were normalized to the maximum value of the transmittance in any given data set. For non-normal incidence measurements, the sample was rotated about the *y*-axis.


**Near-Field RF Measurements inside the Cavity.** We used a wire antenna that comprised a 4 mm length of a coaxial cable from which the metallic mesh shielding and outer dielectric layer had been removed at one end, so as to expose a short length of the central metallic core. This exposed region can act as a small electric dipole receiver and is thus able to detect local electric fields. The wire antenna was positioned sufficiently close, between 1 and 2 mm, to the SRR array (or bare substrate in the case of the empty cavity measurements) such that it was located within the near-fields around the rings (within the fields of the cavity modes). A lens horn antenna

was used to irradiate the systems, and the magnitude and phase of the transmission between the horn antenna and the wire antenna detector were measured using the VNA as a function of position in the plane of the array/cavity. From these data, the magnitude of the transmission at a given phase for each location was determined, and this transmission is directly related to the electric field strength so that the data shown here provide a proxy for maps of the magnitude of the instantaneous electric field strength (achieved through the use of a polarized electrical antenna as the probe).

**Empty Cavity Measurements.** Our empty cavity measurements made use of a blank substrate to mimic everything about our filled cavity except for the array of SRR metamolecules. To do this, we included in the “empty” cavity a  $300 \times 300$  mm, 1.55 mm thick panel of Rogers 4350B substrate, positioned with one surface at the center of the cavity.

## AUTHOR INFORMATION

### Corresponding Author

William L. Barnes – Department of Physics and Astronomy,  
University of Exeter, Exeter, United Kingdom EX4 4QL;  
 [orcid.org/0000-0002-9474-5534](https://orcid.org/0000-0002-9474-5534); Email: [w.l.barnes@exeter.ac.uk](mailto:w.l.barnes@exeter.ac.uk)

### Authors

Milo Baraclough – Department of Physics and Astronomy,  
University of Exeter, Exeter, United Kingdom EX4 4QL  
Ian R. Hooper – Department of Physics and Astronomy,  
University of Exeter, Exeter, United Kingdom EX4 4QL

Complete contact information is available at:

<https://pubs.acs.org/10.1021/acsphotonics.1c00931>

### Author Contributions

M.B. undertook the experimental work, with input from I.R.H. M.B. undertook the data acquisition and data analysis. All authors contributed significantly to data evaluation, project design, and writing of the manuscript. W.L.B. conceived the project.

### Notes

The authors declare no competing financial interest.

## ACKNOWLEDGMENTS

We would like to acknowledge many valuable discussions with Charlie-Ray Mann and Eros Mariani during the lengthy early stages of this work. We also benefited from the superb technical assistance of Nick Cole and Peter Savage in fabricating some of the essential equipment. We would also like to acknowledge many useful discussions arising from the weekly polaritonic chemistry webinar series, in large part driven by Joel Yuen-Zhou and Wei Xiong at UCSD. We acknowledge financial support from the Engineering and Physical Sciences Research Council (EPSRC) of the United Kingdom, via the EPSRC Centre for Doctoral Training in Metamaterials (Grant No. EP/L015331/1). W.L.B. gratefully acknowledges the support of the European Research Council through project photmat (ERC-2016-AdG-742222: [www.photmat.eu](http://www.photmat.eu)). I.R.H. acknowledges support from the EPSRC and QinetiQ Ltd. via the TEAM-A prosperity partnership (Grant No. EP/R004781/1). Data in support of our findings are available at [10.6084/m9.figshare.16441584](https://doi.org/10.6084/m9.figshare.16441584).

## REFERENCES

- (1) Ebbesen, T. W. Hybrid Light–Matter States in a Molecular and Material Science Perspective. *Acc. Chem. Res.* **2016**, *49*, 2403–2412.
- (2) Feist, J.; Galego, J.; Garcia-Vidal, F. J. Polaritonic Chemistry with Organic Molecules. *ACS Photonics* **2018**, *5*, 205–216.
- (3) Bennett, K.; Kowalewski, M.; Mukamel, S. Novel photochemistry of molecular polaritons in optical cavities. *Faraday Discuss.* **2016**, *194*, 259–282.
- (4) Luk, H. L.; Feist, J.; Toppari, J. J.; Groenhof, G. Multiscale Molecular Dynamics Simulations of Polaritonic Chemistry. *J. Chem. Theory Comput.* **2017**, *13*, 4324–4335.
- (5) Ribeiro, R. F.; Martínez-Martínez, L. A.; Du, M.; Campos-Gonzalez-Angulo, J.; Yuen-Zhou, J. Polariton chemistry: controlling molecular dynamics with optical cavities. *Chemical Science* **2018**, *9*, 6325–6339.
- (6) Yuen-Zhou, J.; Menon, V. M. Polariton chemistry: Thinking inside the (photon) box. *Proc. Natl. Acad. Sci. U. S. A.* **2019**, *116*, 5214–5216.
- (7) Lidzey, D. G.; Bradley, D. D. C.; Virgil, T.; Armitage, A.; Skolnick, M. S.; Walker, S. Room temperature polariton emission from strongly coupled organic semiconductor microcavities. *Phys. Rev. Lett.* **1999**, *82*, 3316–3319.
- (8) Shalabney, A.; George, J.; Hutchison, J.; Pupillo, G.; Genet, C.; Ebbesen, T. W. Coherent coupling of molecular resonators with a microcavity mode. *Nat. Commun.* **2015**, *6*, 5981.
- (9) Simpkins, B. S.; Fears, K. P.; Dressick, W. J.; Spann, B. T.; Dunkelberger, A. D.; Owrutsky, J. C. Spanning Strong to Weak Normal Mode Coupling between Vibrational and Fabry–Pérot Cavity Modes through Tuning of Vibrational Absorption Strength. *ACS Photonics* **2015**, *2*, 1460–1467.
- (10) Dai, S.; et al. Tunable phonon polaritons in atomically thin van der Waals crystals of Boron Nitride. *Science* **2014**, *343*, 1125–1129.
- (11) Pons-Valencia, P.; Alfaro-Mozaz, F. J.; Wiecha, M. M.; Bielek, V.; Dolado, I.; Vélaz, S.; Li, P.; Alonso-González, P.; Casanova, F.; Hueso, L. E.; Martín-Moreno, L.; Hillenbrand, R.; Nikitin, A. Y. Launching of hyperbolic phonon-polaritons in h-BN slabs by resonant metal plasmonic antennas. *Nat. Commun.* **2019**, *10*, 3242.
- (12) Ramezani, M.; Halpin, A.; Fernández-Domínguez, A.; Feist, J.; Rodríguez, S.; Garcia-Vidal, F.; Rivas, J. G. Plasmon-exciton-polariton lasing. *Optica* **2017**, *4*, 31–37.
- (13) Kasprzak, J.; Richard, M.; Kundermann, S.; Baas, A.; Jeamburn, P.; Keeling, J. M. J.; Marchetti, F. M.; Szymanska, M. H.; Andre, R.; Staehli, J. L.; Savona, V.; Littlewood, P. B.; Deveaud, B.; Dang, L. S. Bose–Einstein condensation of exciton polaritons. *Nature* **2006**, *443*, 409–414.
- (14) Vasilevskiy, M.; Santiago-Pérez, D.; Trallero-Giner, C.; Peres, N.; Kavokin, A. Exciton-polaritons in 2D dichalcogenide layers placed in a planar microcavity: tuneable interaction between two Bose–Einstein condensates. *Phys. Rev. B: Condens. Matter Mater. Phys.* **2015**, *92*, 245435.
- (15) Su, R.; Ghosh, S.; Wang, J.; Liu, S.; Diederichs, C.; Liew, T. C. H.; Xiong, Q. Observation of exciton polariton condensation in a perovskite lattice at room temperature. *Nat. Phys.* **2020**, *16*, 301–306.
- (16) Thomas, A.; George, J.; Shalabney, A.; Dryzhakov, M.; Varma, S. J.; Moran, J.; Chervy, T.; Zhong, X.; Devaux, E.; Genet, C.; Hutchison, T. A.; Ebbesen, T. W. Ground-State Chemical Reactivity under Vibrational Coupling to the Vacuum Electromagnetic Field. *Angew. Chem.* **2016**, *128*, 11634–11638.
- (17) Thomas, A.; Lethuillier-Karl, L.; Nagarajan, K.; Vergauwe, R. M. A.; George, J.; Chervy, T.; Shalabney, A.; Devaux, E.; Genet, C.; Moran, J.; Ebbesen, T. W. Tilting a ground-state reactivity landscape by vibrational strong coupling. *Science* **2019**, *363*, 615–619.
- (18) Lather, J.; Bhatt, P.; Thomas, A.; Ebbesen, T. W.; George, J. Cavity Catalysis by Cooperative Vibrational Strong Coupling of Reactant and Solvent Molecules. *Angew. Chem., Int. Ed.* **2019**, *58*, 10635–10638.
- (19) Zhong, X.; Chervy, T.; Wang, S.; George, J.; Thomas, A.; Hutchison, J. A.; Devaux, E.; Genet, C.; Ebbesen, T. W. Non-



Radiative Energy Transfer Mediated by Hybrid Light-Matter States. *Angew. Chem., Int. Ed.* **2016**, *55*, 6202–6206.

(20) Zhong, X.; Chervy, T.; Zhang, L.; Thomas, A.; George, J.; Genet, C.; Hutchison, J. A.; Ebbesen, T. W. Energy Transfer between Spatially Separated Entangled Molecules. *Angew. Chem., Int. Ed.* **2017**, *56*, 9034–9038.

(21) Georgiou, K.; Michetti, P.; Gai, L.; Cavazzini, M.; Shen, Z.; Lidzey, D. G. Control over Energy Transfer between Fluorescent BODIPY Dyes in a Strongly Coupled Microcavity. *ACS Photonics* **2018**, *5*, 258–266.

(22) Orgiu, E.; George, J.; Hutchison, J. A.; Devaux, E.; Dayen, J. F.; Doudin, B.; Stellacci, F.; Genet, C.; Schachenmayer, J.; Genes, C.; Pupillo, G.; Samori, P.; Ebbesen, T. W. Conductivity in organic semiconductors hybridized with the vacuum field. *Nat. Mater.* **2015**, *14*, 1123–1129.

(23) Feist, J.; Garcia-Vidal, F. J. Extraordinary Exciton Conductance Induced by Strong Coupling. *Phys. Rev. Lett.* **2015**, *114*, 196402.

(24) Wang, S.; Mika, A.; Hutchison, J. A.; Genet, C.; Jouaiti, A.; Hosseini, M. W.; Ebbesen, T. W. Phase transition of a perovskite strongly coupled to the vacuum field. *Nanoscale* **2014**, *6*, 7243–7248.

(25) Graf, A.; Tropsch, L.; Zakharko, Y.; Zaumseil, J.; Gather, M. C. Near-infrared exciton-polaritons in strongly coupled single-walled carbon nanotube microcavities. *Nat. Commun.* **2016**, *7*, 13078.

(26) Shahnazaryan, V. A.; Saroka, V. A.; Shelykh, I. A.; Barnes, W. L.; Portnoi, M. E. Strong Light–Matter Coupling in Carbon Nanotubes as a Route to Exciton Brightening. *ACS Photonics* **2019**, *6*, 904–914.

(27) Polak, D.; et al. Manipulating molecules with strong coupling: harvesting triplet excitons in organic exciton microcavities. *Chem. Sci.* **2020**, *11*, 343–354.

(28) Houdré, R.; Stanley, R.; Oesterle, U.; Ilegems, M.; Weisbuch, C. Room temperature exciton-photon Rabi splitting in a semiconductor microcavity. *J. Phys. IV* **1993**, *3*, 51–58.

(29) Skolnick, M. S.; Fisher, T. A.; Whittaker, D. M. Strong coupling phenomena in quantum microcavity structures. *Semicond. Sci. Technol.* **1998**, *13*, 645–669.

(30) Vurgaftman, I.; Simpkins, B. S.; Dunkelberger, A. D.; Owrutsky, J. C. Negligible Effect of Vibrational Polaritons on Chemical Reaction Rates via the Density of States Pathway. *J. Phys. Chem. Lett.* **2020**, *11*, 3557–3562.

(31) Imperatore, M. V.; Asbury, J. B.; Giebink, N. C. Reproducibility of cavity-enhanced chemical reaction rates in the vibrational strong coupling regime. *J. Chem. Phys.* **2021**, *154*, 191103.

(32) Stangl, T.; Wilhelm, P.; Remmerssen, K.; Höger, S.; Vogelsang, J.; Lupton, J. M. Mesoscopic quantum emitters from deterministic aggregates of conjugated polymers. *Proc. Natl. Acad. Sci. U. S. A.* **2015**, *112*, E5560–E5566.

(33) Chen, S.; Liu, J.; Lu, H.; Wang, Q.; Zhu, Y. Strong coupling effects between a meta-atom and MIM nanocavity. *AIP Adv.* **2012**, *2*, 032186.

(34) Luxmoore, I. J.; Liu, P. Q.; Li, P.; Faist, J.; Nash, G. R. Graphene–Metamaterial Photodetectors for Integrated Infrared Sensing. *ACS Photonics* **2016**, *3*, 936–941.

(35) Kakuyanagi, K.; Matsuzaki, Y.; Déprez, C.; Toida, H.; Semba, K.; Yamaguchi, H.; Munro, W. J.; Saito, S. Observation of Collective Coupling between an Engineered Ensemble of Macroscopic Artificial Atoms and a Superconducting Resonator. *Phys. Rev. Lett.* **2016**, *117*, 210503.

(36) Yoshihara, F.; Fuse, T.; Ashhab, S.; Kakuyanagi, K.; Saito, S.; Semba, K. Characteristic spectra of circuit quantum electrodynamics systems from the ultrastrong- to the deep-strong-coupling regime. *Phys. Rev. A: At., Mol., Opt. Phys.* **2017**, *95*, 053824.

(37) Meinzer, N.; Barnes, W. L.; Hooper, I. R. Plasmonic meta-atoms and metasurfaces. *Nat. Photonics* **2014**, *8*, 889–898.

(38) Vaskin, A.; Kolkowski, R.; Koenderink, A. F.; Staude, I. Light-emitting metasurfaces. *Nanophotonics* **2019**, *8*, 1151–1198.

(39) Baraclough, M.; Seetharaman, S. S.; Hooper, I. R.; Barnes, W. L. Metamaterial Analogues of Molecular Aggregates. *ACS Photonics* **2019**, *6*, 3003–3009.

(40) Rustomji, K.; Dubois, M.; Kuhlmeier, B.; de Sterke, C. M.; Enoch, S.; Abdeddaim, R.; Wenger, J. Direct Imaging of the Energy-Transfer Enhancement between Two Dipoles in a Photonic Cavity. *Phys. Rev. X* **2019**, *9*, 011041.

(41) Hesmer, F.; Tatartschuk, E.; Zhuromskyy, O.; Radkovskaya, A. A.; Shamonin, M.; Hao, T.; Stevens, C. J.; Faulkner, G.; Edwards, D. J.; Shamonina, E. Coupling mechanisms for split ring resonators: Theory and experiment. *Phys. Status Solidi B* **2007**, *244*, 1170–1175.

(42) Hobson, P. A.; Barnes, W. L.; Lidzey, D. G.; Gehring, G. A.; Whittaker, D. M.; Skolnick, M. S.; Walker, S. Strong exciton–photon coupling in a low-Q all-metal mirror microcavity. *Appl. Phys. Lett.* **2002**, *81*, 3519–3521.

(43) Schwartz, T.; Hutchison, J. A.; Genet, C.; Ebbesen, T. W. Reversible Switching of Ultrastrong Light-Molecule Coupling. *Phys. Rev. Lett.* **2011**, *106*, 196405.

(44) Muallem, M.; Palatnik, A.; Nessim, G. D.; Tischler, Y. R. Strong Light-Matter Coupling and Hybridization of Molecular Vibrations in a Low-Loss Infrared Microcavity. *J. Phys. Chem. Lett.* **2016**, *7*, 2002–2008.

(45) Tropsch, L.; Gather, M. C. Investigating the Onset of the Strong Coupling Regime by Fine-Tuning the Rabi Splitting in Multilayer Organic Microcavities. *Adv. Opt. Mater.* **2018**, *6*, 1800203.

(46) Pendry, J. B.; Holden, A. J.; Robbins, D. J.; Stewart, W. J. Magnetism from conductors and enhanced nonlinear phenomena. *IEEE Trans. Microwave Theory Tech.* **1999**, *47*, 2075–2084.

(47) Savona, V.; Tassone, F. Exact quantum calculation of polaron dispersion in semiconductor microcavities. *Solid State Commun.* **1995**, *95*, 673–678.

(48) Thomas, P. A.; Tan, W. J.; Fernandez, H. A.; Barnes, W. L. A new signature for strong light-matter coupling using spectroscopic ellipsometry. *Nano Lett.* **2020**, *20*, 6412–6419.

(49) Bajoni, D. Polariton lasers. Hybrid light-matter lasers without inversion. *J. Phys. D: Appl. Phys.* **2012**, *45*, 313001.

(50) Ujihara, K. Spontaneous emission and the concept of effective area in a very short optical cavity with plane-parallel dielectric mirrors. *Jpn. J. Appl. Phys.* **1991**, *30*, L901–L903.

(51) Rodriguez, S. R. K.; Murai, S.; Verschuuren, M. A.; Rivas, J. G. Light-Emitting Waveguide-Plasmon Polaritons. *Phys. Rev. Lett.* **2012**, *109*, 166803.

(52) Houdré, R.; Stanley, R. P.; Ilegems, M. Vacuum-field Rabi splitting in the presence of inhomogeneous broadening: resolution of a homogeneous linewidth in an inhomogeneously broadened system. *Phys. Rev. A: At., Mol., Opt. Phys.* **1996**, *53*, 2711–2715.

(53) Scholes, G. D. Polaritons and excitons: Hamiltonian design for enhanced coherence. *Proc. R. Soc. London, Ser. A* **2020**, *476*, 20200278.

(54) Botzung, T.; Hagenmüller, D.; Schütz, S.; Dubail, J.; Pupillo, G.; Schachenmayer, J. Dark state semilocalization of quantum emitters in a cavity. *Phys. Rev. B: Condens. Matter Mater. Phys.* **2020**, *102*, 144202.

(55) Du, M.; Yuen-Zhou, J. Can Dark States Explain Vibropolaritonic Chemistry? 2021, arxiv.org/abs/2104.07214. <https://arxiv.org/abs/2104.07214> (accessed 2021-08-25).

(56) Törmä, P.; Barnes, W. L. Strong coupling between surface plasmon polaritons and emitters: a review. *Rep. Prog. Phys.* **2015**, *78*, 013901.

(57) Thomas, P. A.; Menghrajani, K. S.; Barnes, W. L. Cavity-Free Ultrastrong Light-Matter Coupling. *J. Phys. Chem. Lett.* **2021**, *12*, 6914–6918.

(58) Seetharaman, S. S.; King, C. G.; Hooper, I. R.; Barnes, W. L. Electromagnetic interactions in a pair of coupled split-ring resonators. *Phys. Rev. B: Condens. Matter Mater. Phys.* **2017**, *96*, 085426.

(59) Sersic, I.; Frimmer, M.; Verhagen, E.; Koenderink, A. F. Electric and Magnetic Dipole Coupling in Near-Infrared Split-Ring Metamaterial Arrays. *Phys. Rev. Lett.* **2009**, *103*, 213902.